X-Ray Spectroscopy Diagnostics with XMM: New Prospects for the Physics of Thermal, Optically Thin Plasmas

M. Güdel[1], R. Mewe[2]
A. C. Brinkman[2], J. S. Kaastra[2], F. B. S. Paerels[2], S. M. Kahn[3], A. Rasmussen[3], L. K. Harra-Murnion[4]

ABSTRACT

We present feasibility studies based on extensive simulations of the XMM X-ray instruments, in particular the Reflection Grating Spectrometer.

1. Introduction

XMM will open new windows for plasma diagnostics over a wide range of physical conditions. We simulated the performance of the two Reflection Grating Spectrometer modules (RGS; 0.35–2.5 keV, effective area ~ 150 cm^2) and the three European Photon Imaging Camera modules (EPIC; 0.1–10 keV). The simulations are based on analytical response matrices that accurately model the wavelength-dependent effective areas and point-spread functions. They were carried out with the Utrecht spectral code SPEX (Kaastra, Mewe, & Nieuwenhuijzen 1996) with up-to-date spectral models for lines and continua of thermal plasmas in ionization equilibrium, including realistic Poisson noise. Characteristic examples are shown in Figure 1 (Capella, exposure time = 20 ks).

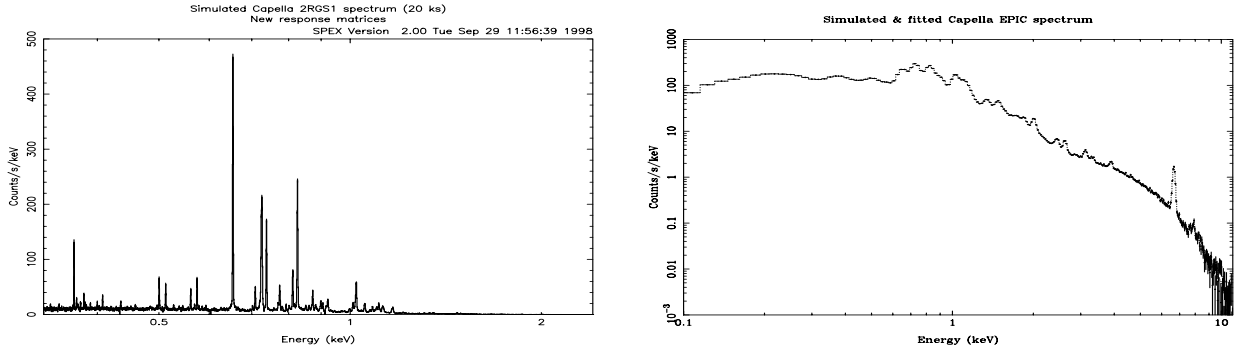

Fig. 1.— Simulated (crosses) and fitted (histogram) RGS and EPIC spectra of Capella (20 ks).

[1]Paul Scherrer Institute, 5232 Villigen PSI, Switzerland

[2]SRON, 3584 CA Utrecht, The Netherlands

[3]Columbia Astrophysics Laboratory, New York, USA

[4]MSSL, Dorking, UK

Table 1: 2-T/abundance fits for Capella (model 1), 20 ks (14.3 cts s^{-1} per 2 RGS) and for EK Dra (model 2), 70 ks (0.48 cts s^{-1} per 2 RGS)

	T_1(keV)	T_2(keV)	$EM_1(10^{50})$	$EM_2(10^{50})$	Fe	Mg	Si	O
model 1	0.430	2.16	5.00	15.00	0.800	1.20	0.800	0.800
fit RGS	0.428	2.16	5.03	14.9	0.80	1.21	0.75	0.79
error	±0.002	±0.02	±0.06	±0.1	±0.01	±0.04	±0.04	±0.01
fit EPIC	0.431	2.158	4.99	15.01	0.800	1.18	0.807	0.803
error	±0.001	±0.004	±0.02	±0.03	±0.004	±0.02	±0.014	±0.005
model 2	0.600	1.98	1.60	1.00	0.83	1.69	1.00	1.00
fit RGS	0.603	1.95	1.58	0.96	0.85	1.69	1.15	1.02
error	±0.003	±0.11	±0.06	±0.07	±0.04	±0.12	±0.16	±0.05
fit EPIC	0.599	1.97	1.60	1.01	0.829	1.66	1.04	1.00
error	±0.001	±0.03	±0.02	±0.02	±0.009	±0.04	±0.04	±0.02

2. Temperatures, Emission Measures, and Elemental Abundances

Table 1 shows recovered temperatures T, emission measures (EM in 10^{50} cm^{-3}) and a few abundances (relative to solar photospheric; Anders & Grevesse 1989) for two exemplary two-component plasmas, representative for the coronae of Capella and EK Dra, respectively. The input *model* is compared with the recovered *fit* values. Errors are $\chi^2 + 2$ errors. Thus, for typical sources, these parameters are recovered at the few-percent level. We further simulated the EM distribution of the solar-type star EK Dra (≈ 0.48 cts s^{-1} for two RGS; Güdel et al. 1997). The EM distribution was recovered from spectra simulated for various exposure times (Fig. 2).

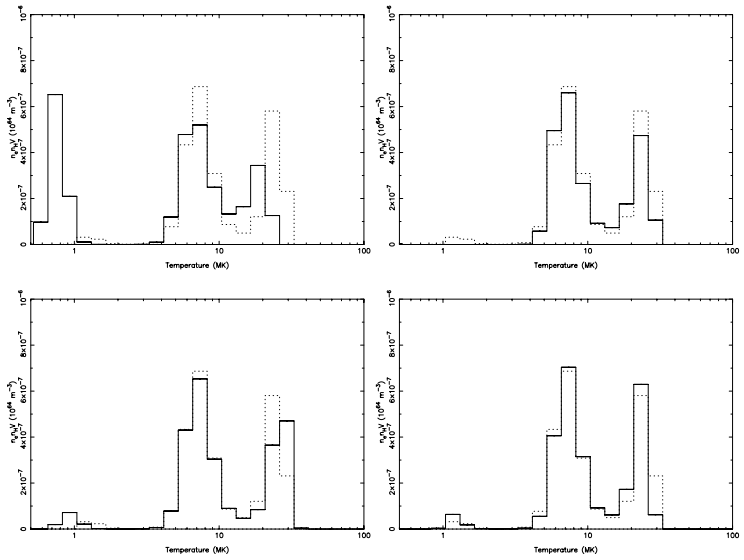

Fig. 2.— EM distribution reconstruction for EK Dra. The dotted line describes the input EM distribution, the solid histograms are the fit results. *Top left:* exposure time of 10 ks; *top right:* 20 ks; *bottom left:* 30 ks; *bottom right:* 50 ks.

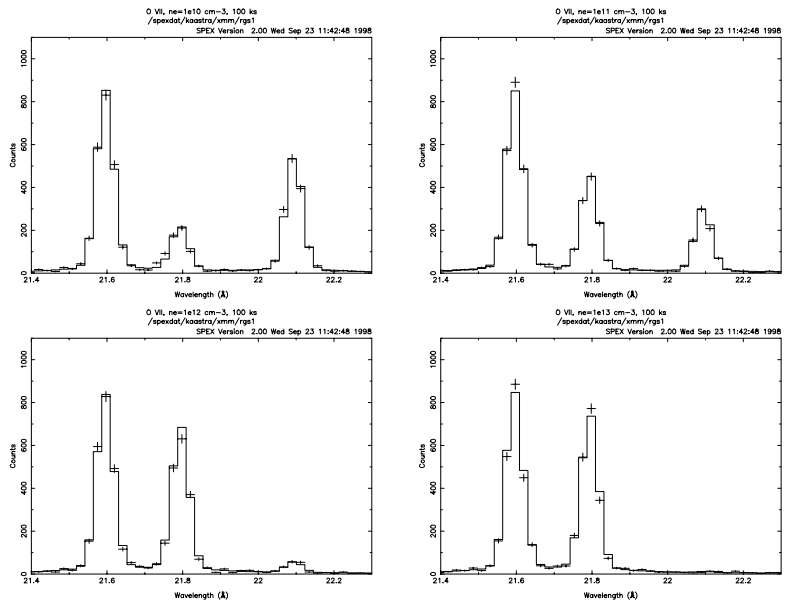

Fig. 3.— RGS simulations and fits of the O VII triplet. Electron densities are 10^{10} cm^{-3} (upper left), 10^{11} cm^{-3} (upper right), 10^{12} cm^{-3} (lower left), and 10^{13} cm^{-3} (lower right).

3. Density Diagnostics

Our electron density diagnostics is based on the line flux ratios of the helium-like triplets of O VII (Fig. 3), Ne IX, Mg XI, and Si XIII which are also temperature-sensitive. This results in some bias for good diagnostics toward cool plasmas (2–5 MK) at lower densities ($10^9 - 10^{13}$ cm^{-3}) or hot plasmas ($\gtrsim$ 5 MK) at high densities ($\gtrsim 10^{12}$ cm^{-3}; e.g., Mewe, Lemen & Schrijver 1991). The plots in Figure 4 show recovered densities using input densities of $10^9, 10^{10}, 10^{11}, 10^{12}$, 10^{13}, 10^{14}, and 10^{15} cm^{-3}, with different exposure times for two RGS modules. The assumed temperatures correspond to the formation temperatures of O VII, Ne IX, Mg XI, and Si XIII, respectively. The recovered values and their error bars ($\chi^2 + 2$ errors) are identified with different symbols for different input densities and obviously converge to the input value (horizontal lines) for long enough exposure times. The x-axis is given as the product of exposure time (ks) $\times$ EM ($/10^{51}$cm^{-3}) $\times$ (10 pc/distance)$^{-2}$. The upper x-axis scale indicates the total number of counts collected by the two RGS. See also Table 2 for a realistic simulation of Capella.

Table 2: Density diagnostics for Capella, 20 ks; electron density n_e in units of 10^{10} cm^{-3}

density	0.10	1.00	10.0	100	10^3	10^4	10^5
fit RGS	< 0.17	1.20 ± 0.41	10.0 ± 1.1	108 ± 12	1.01 ± 0.13 $\times 10^3$	1.15 ± 0.34 $\times 10^4$	$0.41^{+0.32}_{-0.15}$ $\times 10^5$
fit EPIC	—	—	$7.6^{+10.2}_{-5.1}$	128 ± 104	1.55 ± 0.53 $\times 10^3$	0.85 ± 0.18 $\times 10^4$	$1.07^{+1.85}_{-0.54}$ $\times 10^5$

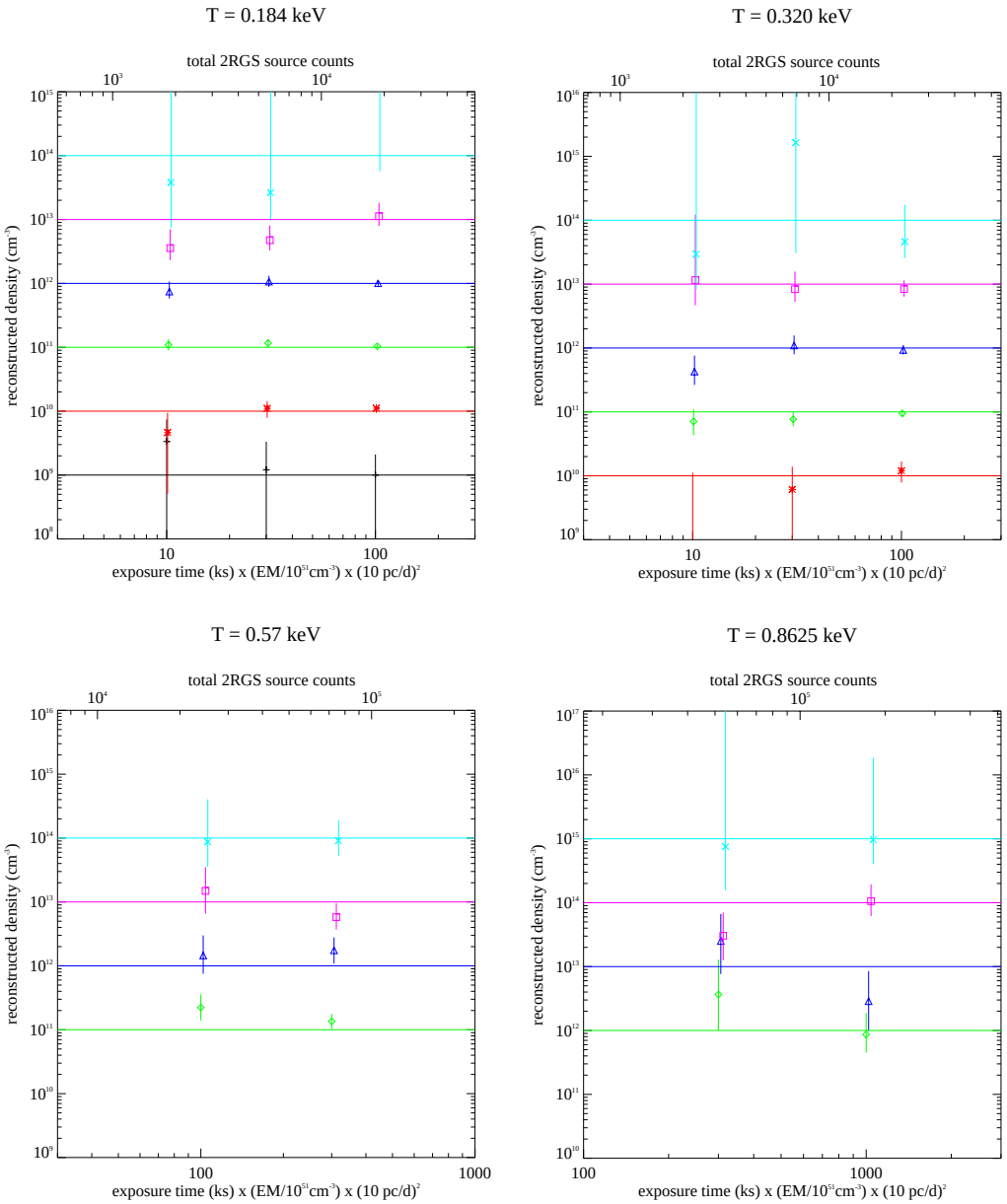

Fig. 4.— RGS reconstruction quality of densities at a given temperature (indicated in plot title) for various exposure times, emission measures, and distances (see x-axis label). The horizontal lines indicate input density values, the symbols and error bars show the recovered densities for the input exposure time×EM/distance^2 (see §3 for details).

4. RGS: Velocity Diagnostics

We have performed velocity simulations for the RGS instrument. Two emission measures with relative motion along the line of sight have been assumed. The results are displayed in Figure 5 in a similar fashion as in Figure 4. We have simulated relative velocities v of 90 km s^{-1}, 300 km s^{-1}, and 600 km s^{-1}, assuming $\mathrm{EM}_2/\mathrm{EM}_1 = 1$ or 2, again based on our "standard star" ($\mathrm{EM}_1 = 10^{51}$ cm^{-3}, $T_1 = T_2 = 1$ keV, distance = 10 pc). We normalize v by $c = 3 \times 10^{10}$ cm s^{-1}.

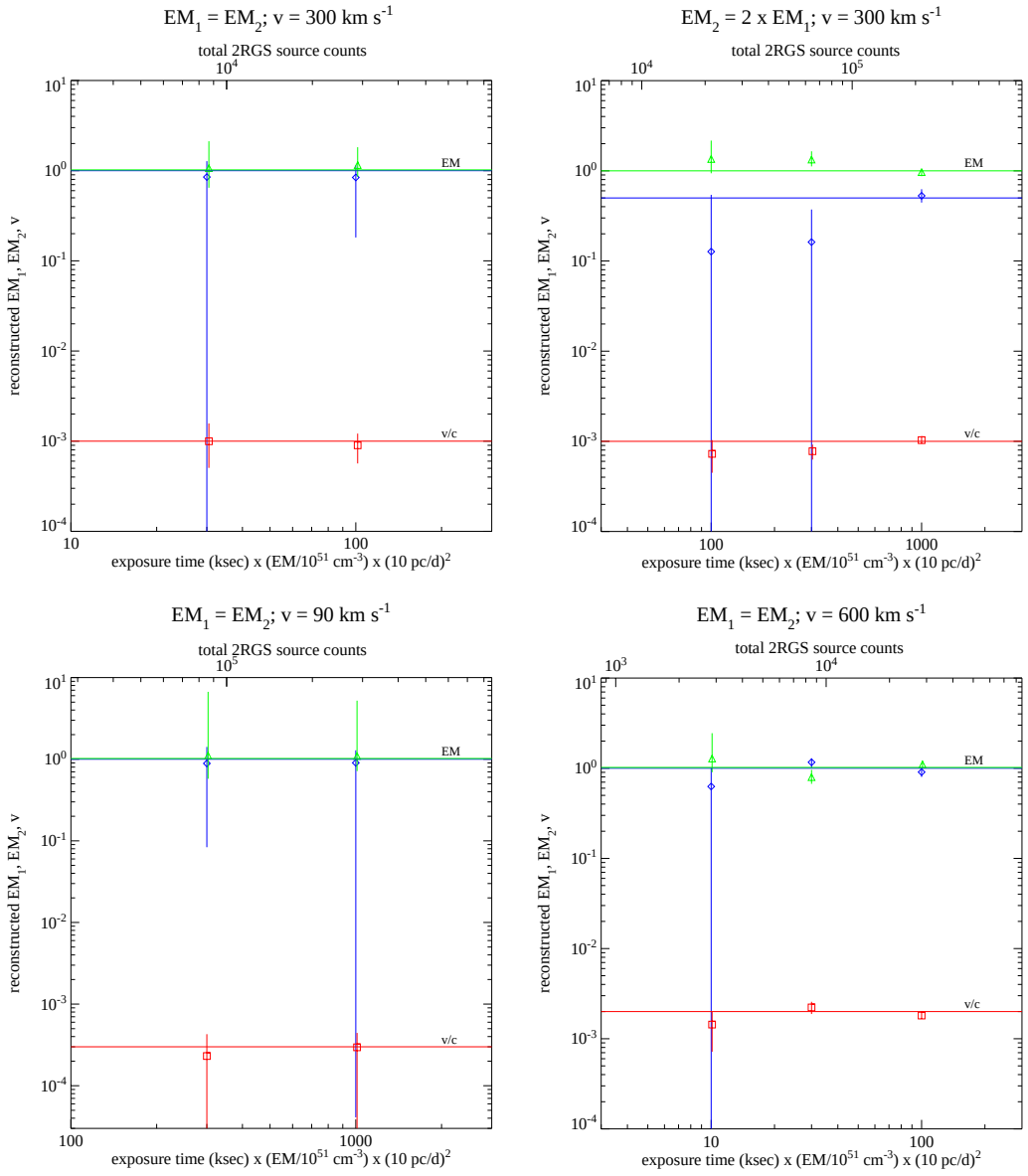

Fig. 5.— RGS velocity diagnostics, see text for details

5. Discussion

We have simulated the performance of the XMM X-ray spectroscopic instruments. The presented simulation results must be interpreted with caution. Not only is the present knowledge of the instruments themselves idealized, but there are well-known deficiencies in the presently available atomic physics data and the ionization balance. Further, the physical state of real astrophysical plasmas is often unknown, e.g., with regard to ionization equilibrium, short-term variations, or inhomogeneities (e.g., abundance patterns in structures with different temperatures). With this in mind, we interpret our results as a test of the idealized instruments that quantifies their performance *if* we had the complete theoretical means to understand the *incident* spectrum. With this proviso, we summarize the simulation results as follows:

- *Temperature, emission measure,* and *abundance* analysis can be well performed with both instruments. Bright objects (order of 1 ct s^{-1} in the RGS) yield relative errors in these parameters typically on the order of 0.5–5% after exposure times of a few tens of ks.
- *EM distribution* reconstructions are easy with the RGS simulated here. For objects with ~ 1 ct s^{-1} in the RGS, a good reconstruction is achieved after about 30 ks of exposure time.
- RGS is excellent for *electron density diagnostics.* Depending on the EM distribution (T-sensitive helium-like triplets used for density diagnostics!), densities can be well reconstructed for the brighter objects with exposure times of the order of 100 ks for 0.3 dex accuracy (or better), in the range $\sim 10^{10} - 10^{14}$ cm^{-3}.
- RGS *velocity diagnostics* resolves relative velocities of 300 km s^{-1} for bright objects (order of 1 ct s^{-1} in the RGS) after exposure times of the order of 100 ks, assuming similar EMs.

In summary, then, there are prospects and challenges in the use of this wonderful satellite that will open a new century of X-ray astronomy. Let us hope that the prospects will be satisfied by the instruments' performance, and the challenges be rewarded by numerous scientific discoveries!

REFERENCES

Anders, E., & Grevesse, N. 1989, Geochim. Cosmochim. Acta, 53, 197

Güdel, M., Guinan, E. F., Mewe, R., Kaastra, J. S., & Skinner, S. L. 1997, ApJ, 479, 416

Kaastra, J. S., Mewe, R., & Nieuwenhuijzen H. 1996, in UV and X-ray spectroscopy of astrophysical and laboratory plasmas, eds. K. Yamashita and T. Watanabe, Univ. Acad. Press, 411

Mewe, R., Lemen, J. R., & Schrijver, C. J. 1991, Ap&SS, 182, 35